De novo phytosterol synthesis in animals

Dolma Michellod[1], Tanja Bien[2], Daniel Birgel[3], Marlene Jensen[4], Manuel Kleiner[4], Sarah Fearn[5], Caroline Zeidler[1], Harald R Gruber-Vodicka[1], Nicole Dubilier[1,6*], Manuel Liebeke[1*]

[1] Max Planck Institute for Marine Microbiology, Celsiusstraße 1, 28359 Bremen, Germany
[2] Institute of Hygiene, University of Münster, Robert-Koch-Str. 41, 48149, Münster, Germany
[3] Institute for Geology, Center for Earth System Research and Sustainability, University of Hamburg, Bundesstraße 55, 20146 Hamburg, Germany
[4] Department of Plant and Microbial Biology NC State University, Raleigh, NC 27695, USA
[5] Department of Materials, Imperial College London, London SW7 2AZ, United Kingdom
[6] MARUM, Center for Marine Environmental Sciences, University of Bremen, 28359 Bremen, Germany

*corresponding authors: mliebeke@mpi-bremen.de, ndubilier@mpi-bremen.de

Abstract

Sterols are lipids that regulate multiple processes in eukaryotic cells, and are essential components of cellular membranes. Sterols are currently assumed to be kingdom specific, with phytosterol synthesis restricted to plants while animals are only able to synthesize cholesterol. Here, we challenge this assumption by demonstrating that the marine annelids *Olavius* and *Inanidrilus* synthesize the phytosterol sitosterol *de novo*. Using multi-omics, high-resolution metabolite imaging, heterologous gene expression and enzyme assays, we show that sitosterol is the most abundant (60%) sterol in these animals and characterize its biosynthetic pathway. We show that phytosterol synthesis partially overlaps with cholesterol synthesis and involves a non-canonical C-24 sterol methyltransferase (C_{24}-SMT). C_{24}-SMT is an essential enzyme for sitosterol synthesis in plants, but not known from animals with bilateral symmetry (bilaterians). Our comparative phylogenetic analyses of C_{24}-SMT homologs revealed that these are

widely distributed across annelids and other animal phyla, including sponges and rotifers. Our findings show that phytosterol synthesis and use is not restricted to the plant kingdom, and indicate that the evolution of sterols in animals is more complex than previously assumed.

Introduction

Sterols are essential lipids present in all eukaryotes. They regulate the physical properties of biological membranes and are involved in the formation of specialized lipid-protein microdomains critical for signal transduction (Yeagle, 1985; Simons & Ikonen, 1997; Simons & Toomre, 2000). In addition, as precursors and cofactors of signaling molecules, they participate in many signaling and regulatory pathways (Chiang & Ferrell, 2020; Radhakrishnan et al., 2020; Sarkar & Chattopadhyay, 2022; Thummel & Chory, 2002). While sterols are ubiquitous in eukaryotes, their distribution is assumed to be kingdom specific: fungi synthesize ergosterol (C_{28}); plants harbor a mixture of phytosterols (C_{28} to C_{29}) dominated by sitosterol, stigmasterol, and campesterol (Lagarda et al., 2006) and animals use cholesterol (C_{27}). These inter-kingdom differences reflect a complex evolutionary history of sterol synthesis. Previous phylogenetic analyses suggest that most enzymes for the biosynthesis of plant, fungal, and animal sterols were already present in the last eukaryotic common ancestor (LECA) (Desmond & Gribaldo, 2009; Summons et al., 2006), with the kingdom-specific distribution observed in extant species then evolving from LECA through multiple events of enzyme losses and specializations.

Kingdom-specific sterols differ from each other in only small structural details. For example, phytosterols differ from cholesterol by the presence of an extra methyl- or ethyl-group at position C_{24}. This methylation is catalyzed by C_{24} sterol methyltransferase (C_{24}-SMT), an enzyme widely distributed in plants, protists and fungi but absent in nearly all animals (Haubrich et al., 2015; Volkman, 2005). The only exception are some marine sponges, in which C_{24}-SMT homologues are not related to phytosterol synthesis but assumed to participate in the synthesis of 24-isopropylcholesterol, a cholesterol derivative that serves as a sponge biomarker (Germer et al., 2017; Gold et al., 2016).

As with most other sterol enzymes, an ancestral C_{24}-SMT was likely present in the LECA but lost early in the evolution of animals, probably after the divergence of sponges, explaining why this enzyme is absent from bilaterians and why animals lack the ability to produce phytosterols (Desmond & Gribaldo, 2009; Gold et al., 2016; Haubrich et al., 2015).

Here, we show that phytosterol biosynthesis and use is not restricted to plants. By screening multiple members of a globally distributed group of marine gutless annelids from the genera *Olavius* and *Inanidrilus*, we show that all eight species analyzed have sitosterol as their main sterol and express the genes needed for its synthesis. We characterized the sitosterol biosynthetic pathway used by these annelids and demonstrate the importance of a previously uncharacterized group of C_{24}-SMT homologs encoded in these animals' genomes. Using heterologous gene expression and enzymatic assays, we show that two animal C_{24}-SMT homologs are functional and catalyzes both C-24 and C-28 methylations. Finally, we discovered that C_{24}-SMT homologs are widely distributed across annelids and other animal phyla, including sponges and rotifers, suggesting that phytosterols may also be synthesized by other animals Our findings demonstrate that animals are capable of synthesizing and using phytosterol and that these molecules are not restricted to the plant kingdom, and suggest that the use of phytosterols as geological biomarkers for plants should be reconsidered

Results and discussion

Sitosterol is the main sterol in the marine gutless annelid *Olavius algarvensis*

O. algarvensis belongs to a group of gutless marine annelids that are found worldwide, mainly in coral-reef and seagrass sediments. These annelids lack a digestive system and are obligately associated with bacterial endosymbionts that provide them with nutrition (Giere, 1981, 1985; Kleiner et al., 2012; Woyke et al., 2006). As part of our ongoing efforts to characterize the *O. algarvensis* symbiosis, we analyzed the metabolome of single worm individuals using both gas chromatography-mass

spectrometry (GC-MS) and high-performance liquid chromatography-mass spectrometry (HPLC-MS). These analyses revealed an unusual sterol composition, with sitosterol accounting for the majority of the sterols detected (60%), and the remainder consisting of cholesterol (**Figure 1A**). This was unexpected, as cholesterol usually dominates the sterol pool in bilaterians, often making up more than 90% of the total sterol content (Goad, 1981; Sissener et al., 2018). Sitosterol is a phytosterol and, among bilaterians, has only been reported as the most abundant sterol in a few phytoparasitic nematodes that are incapable of *de novo* sterol synthesis (Chitwood et al., 1985, 1987; Cole & Krusberg, 1967). In these plant parasites, it is unclear if the detected phytosterol is only present in the nematode gut content, or incorporated into their cells and tissue**.** The absence of a gut in *O. algarvensis* excludes sterol contamination from plant matter in the digestive tract. However, sitosterol could originate from the bacterial symbionts of *O. algarvensis*, which form a thick layer between the cuticle and the epidermis of the animal (**Figure 1B**).

To investigate this possibility, we used two high spatial-resolution metabolite imaging techniques to localize the two major sterols in *O. algarvensis.* Time-of-Flight Secondary Ion Mass Spectrometry (TOF-SIMS) data revealed that, at a spatial resolution of 0.4 µm, both sitosterol and cholesterol were uniformly distributed throughout the animals' tissues (**Figure 1C and 1D**). We found no evidence for a tissue-specific distribution of these two sterols, that is, there was no correlation between symbiont location and sitosterol distribution. These findings are supported by a second mass spectrometry imaging method, matrix-assisted laser desorption ionization mass spectrometry imaging (MALDI-2-MSI), of cross and longitudinal sections at a spatial resolution of 5 µm. The MALDI imaging data of longitudinal worm sections confirmed a uniform distribution of sitosterol and cholesterol throughout the animal (**Supplementary Figure 1 and 2**) and the identity of these sterols (**Supplementary Table 1).** This homogeneous sterol distribution sterols suggests that the bacterial symbionts are not the source for phytosterol in *O. algarvensis*.

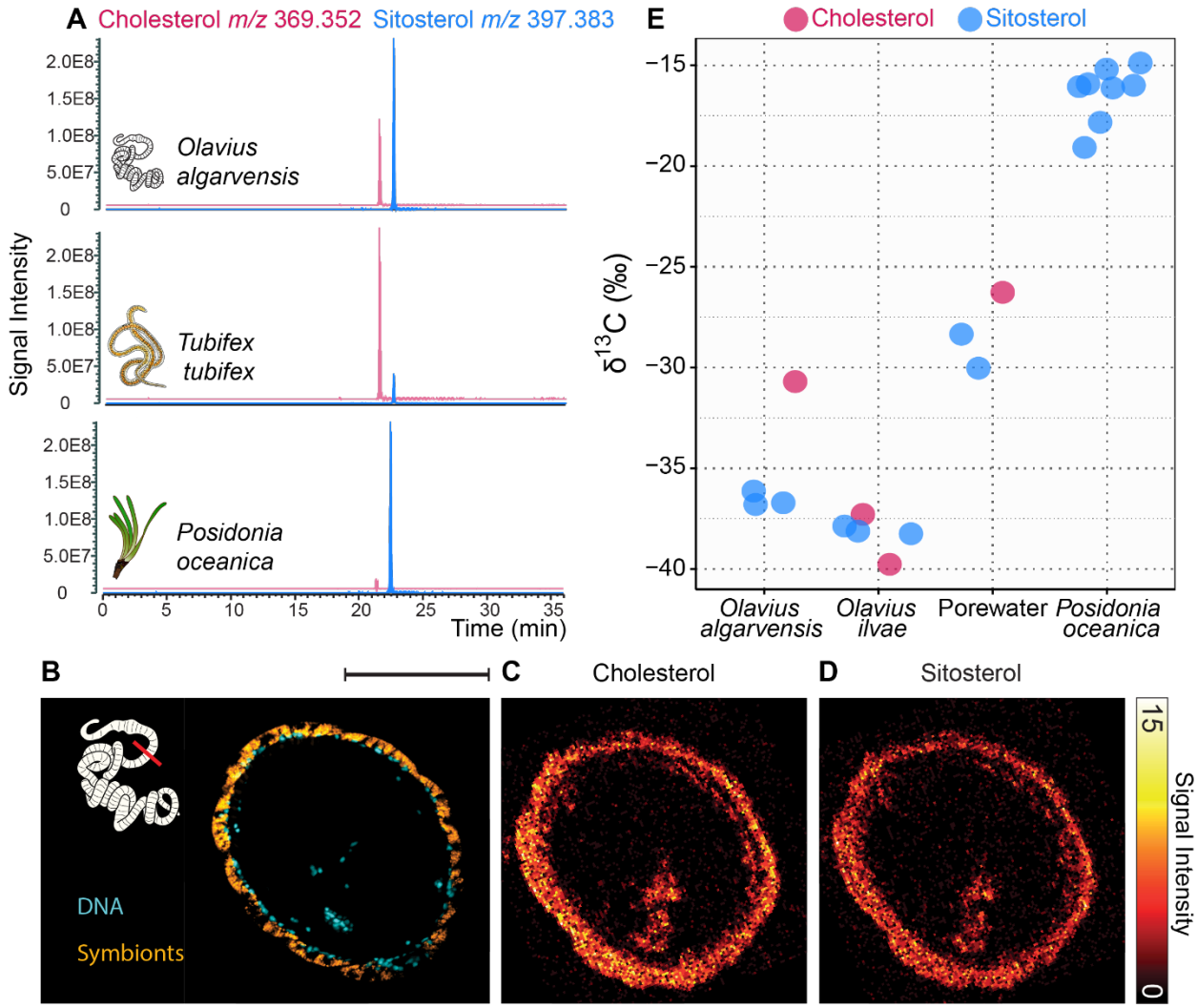

Figure 1 | *Olavius algarvensis* has an unusual sterol profile dominated by sitosterol, a plant sterol. **A**, Extracted-ion chromatograms (XIC) of cholesterol ($[M-H_2O+H]^+$ $C_{27}H_{45}$ at *m/z* 369.352 (red)) and sitosterol ($[M-H_2O+H]^+$ $C_{29}H_{49}$ at *m/z* 397.383 (blue)). The XICs were generated from lipid extracts of (from top to bottom): the gutless marine annelid *O. algarvensis*, the freshwater annelid *Tubifex tubifex,* and the seagrass *Posidonia oceanica*. **B**, Chemosynthetic symbiotic bacteria are located just below the cuticle of *O. algarvensis.*16S rRNA fluorescence *in situ* hybridization (FISH) image of a cross section through a worm showing the symbionts in yellow (general eubacterial probe) and host nuclei in blue (DAPI). **C and D**, Distribution of sitosterol and cholesterol in *O. algarvensis* measured by TOF-SIMS **C**, Summed intensity of cholesterol ions (*m/z* 369.38, 385.34, 401.35) measured with TOF-SIMS. **D**, Summed intensity of sitosterol ions (*m/z*: 397.47, 383.37, 413.45) as measured by TOF-SIMS. **E**, The ^{13}C isotopic composition of sterols in gutless annelids differed from that of the neighboring seagrass (*P. oceanica*) and sediment porewater. Scale bar in **B-D** 100 µm.

O. algarvensis sterols have an isotopic composition that is distinct from their environment

Having found no evidence based on sterol distribution for a bacterial origin of sitosterol in *O. algarvensis*, we investigated if these animals acquire their sterols from the

129 environment. Chemical analyses of porewater collected in the vicinity of seagrass
130 meadows, the habitat of many gutless annelids (including *O. algarvensis*), showed that
131 sterols were present in the environment in concentrations sufficient to sustain the
132 growth of small sterol-auxotrophic invertebrates (**Supplementary information and**
133 **Supplementary Figure 3**). Therefore, we further investigated the origin of sterols in *O.*
134 *algarvensis* by analyzing the carbon isotopic signature ($\delta^{13}C$) of sterols in the worms,
135 their environment (which includes the seagrass *Posidonia oceanica*) and the porewater
136 of the sediments these worms live in. Carbon isotopic signatures are used to reveal
137 carbon sources and their paths through the food web. As a rule, the bulk $\delta^{13}C$ values of
138 animals reflect their dietary sources (0.5 ‰ to 2 ‰ difference) (McCutchan et al., 2003;
139 Tiunov, 2007). The $\delta^{13}C$ values of sterols are depleted in ^{13}C relative to bulk biomass by
140 5 ‰ to 8 ‰ (Canuel et al., 1997; Hayes, 2018). Results from gas chromatography
141 isotope ratio mass spectrometry (GC-IRMS) with single metabolite resolution showed
142 that sitosterol in the seagrass and porewater had $\delta^{13}C$ values ranging from −30 ‰ to
143 −15 ‰ (**Figure 1E and Supplementary information**). The sterols in *O. algarvensis*, as
144 well as those in another co-occurring gutless annelid species, *Olavius ilvae*, had much
145 lower $\delta^{13}C$ values: −38 ‰ to −36 ‰ for sitosterol and −40 ‰ to −31 ‰ for cholesterol
146 (**Figure 1E**). The difference in the isotopic signature of sterols in both *Olavius* species
147 and their environment excludes that these worms acquired sterols from their
148 environment, and instead indicates an endogenous origin. *O algarvensis*, as all other
149 *Olavius* and *Inanidrilus* species, derives all of its nutrition from its chemosynthetic
150 bacterial symbionts, and this is reflected in its bulk isotopic composition with $\delta^{13}C$ values
151 of −30.6 ‰ (Kleiner et al., 2015). The ^{13}C-depleted signatures of both cholesterol and
152 sitosterol by 1 to 10 ‰ compared to bulk biomass in *O. algarvensis* and *O. ilvae* led us
153 to hypothesize that these animals synthesize both sterols *de novo*, using organic carbon
154 derived from their chemosynthetic symbionts.

155 ***O. algarvensis* encodes and expresses enzymes involved in sitosterol synthesis**
156 **that overlap with those of cholesterol synthesis**

157 Having ruled out an external, environmental source of sitosterol in *O. algarvensis*, we
158 next investigated if the animals themselves can synthesize this phytosterol. To identify

159 and characterize the biosynthetic pathways involved in sterol production, we sequenced
160 and assembled the genome of *O. algarvensis* and analyzed metatranscriptomic and
161 metaproteomic data to search for enzymes involved in *de novo* sterol synthesis,
162 screening both *O. algarvensis* and its symbionts. These analyses revealed that the
163 symbionts, as most bacteria, do not encode enzymes involved in sterol synthesis. The
164 host, on the other hand, possessed the full enzymatic toolbox required for cholesterol
165 synthesis, with homologs of the 11 enzymes present in the genome of *O. algarvensis*
166 (**Supplementary Figure 4 and Supplementary Table 2**). The cholesterol biosynthesis
167 pathway, starting with squalene, is a series of ten connected enzymatic reactions
168 encoded by 11 genes (**Supplementary Figure 4 and Supplementary Table 3**).
169 Homologs of all enzymes were transcribed (11 out of 11 enzymes) and many of the
170 proteins were detected in the proteome of *O. algarvensis* (5 out of 11 proteins)
171 (**Supplementary Figure 4 and Supplementary Tables 4 and 5**), indicating active
172 expression of the genes involved in cholesterol synthesis. Phylogenetic analysis
173 allowed us to assign each homolog to an ortholog group and thus to a potential function
174 (**Supplementary Figures 5 to 14**). Collectively, these data show that *O. algarvensis*
175 has all the enzymes required for *de novo* cholesterol synthesis, which in combination
176 with the isotopic signature of their cholesterol, suggests that these worms are able to
177 synthesize cholesterol.

178 More importantly, our analyses also identified a homolog of C_{24}-SMT, an enzyme
179 essential to sitosterol synthesis, in the genome of *O. algarvensis* (**Figure 2**). As
180 described above, bilaterians are thought to lack C_{24}-SMT. C_{24}-SMT catalyzes the
181 transfer of a methyl group from S-adenosyl-L-methionine (SAM) to the sterol side chain
182 and is essential for the biosynthesis of plant sterols. The gene structure of the putative
183 C_{24}-SMT confirmed its eukaryotic origin and excluded bacterial contamination (**Figure**
184 **2**). The putative C_{24}-SMT gene is a 1071 bp open reading frame (ORF) encoding a 356
185 amino-acid polypeptide (**Supplementary Table 3**), and contains all the conserved
186 residues characteristic of C_{24}-SMT as well as the four conserved signature motifs
187 responsible for substrate binding (**Supplementary Figure 15**) (Bouvier-Navé et al.,
188 1998; Jayasimha & Nes, 2008; Nes et al., 2004, 2008; Nes & Heupel, 1986; Schaller,
189 2004; Veeramachaneni, P. P., 2005). We identified the C_{24}-SMT gene in *O. algarvensis*

190 transcriptomes and proteomes, confirming that these animals express this enzyme
191 **(Figure 2, Supplementary Table 4 and 5**). Our findings suggest that the *O. algarvensis*
192 C_{24}-SMT gene encodes a functional enzyme that may be involved in sitosterol
193 metabolism in these annelids, and represents the first discovery of a C_{24}-SMT enzyme
194 in bilaterians.

195 **The *O. algarvensis* C_{24}-SMT homolog is bifunctional and consecutively transfers**
196 **methyl groups to sterol intermediates**

197 Two methylation reactions are required for the final steps of sitosterol synthesis, one that
198 adds a methyl group at C-24 and one at C-28. These reactions can be catalyzed by the
199 same or different enzymes. For example, in most plants, C-24 and C-28 methylations are
200 mediated by different enzyme isoforms, SMT1 and SMT2 (Bouvier-Navé et al., 1998;
201 Hartmann, 2004; Neelakandan et al., 2009). Alternatively, in basal plants such as green
202 algae, a single C_{24}-SMT catalyzes both methylation steps, (Desmond & Gribaldo, 2009;
203 Haubrich et al., 2015). Sterol profiles and genome analyses of sponges, where C_{24}-SMTs
204 participate in the synthesis of the cholesterol derivative 24-isopropylcholesterol, suggest
205 that these enzymes are similarly bifunctional, although their biochemical activity remains
206 to be characterized (Gold et al., 2016). Since *O. algarvensis* encodes a single C_{24}-SMT
207 homolog, we hypothesized that this enzyme mediates both C-24 and C-28 methylation.
208
209 To test this hypothesis, we overexpressed *O. algarvensis* C_{24}-SMT in *Escherichia coli*
210 and examined its enzymatic activity, substrate preferences, and products by assaying
211 crude protein extracts with a methyl-donor (S-adenosylmethionine, SAM) and different
212 sterol substrates. The C_{24}-SMT from *O. algarvensis* expressed in *E. coli* was not able to
213 methylate classical plant sterol substrates (**Supplementary Table 14)**. However, the
214 enzyme was able to methylate zymosterol and desmosterol, two intermediates of the
215 cholesterol biosynthetic pathway. When incubated with either of these sterol substrates
216 and SAM, the *O. algarvensis* C_{24}-SMT produced a methylated C_{28} product (**Figure 2**
217 **and Supplementary Figure 16-19**). Zymosterol was methylated to fecosterol and
218 desmosterol to 24-methylene-cholesterol. The shift in retention times and changes in
219 mass spectra of the products indicated that a methyl group was added to their sterol

side chain, likely at the C_{24}-position (**Supplementary Figure 18-19**). These results suggest that the cholesterol and sitosterol synthesis pathways overlap in *O. algarvensis*, as the two C_{24}-SMT substrates, zymosterol and desmosterol, are intermediates produced in the second half of the animal cholesterol synthesis pathway (**Figure 2**).

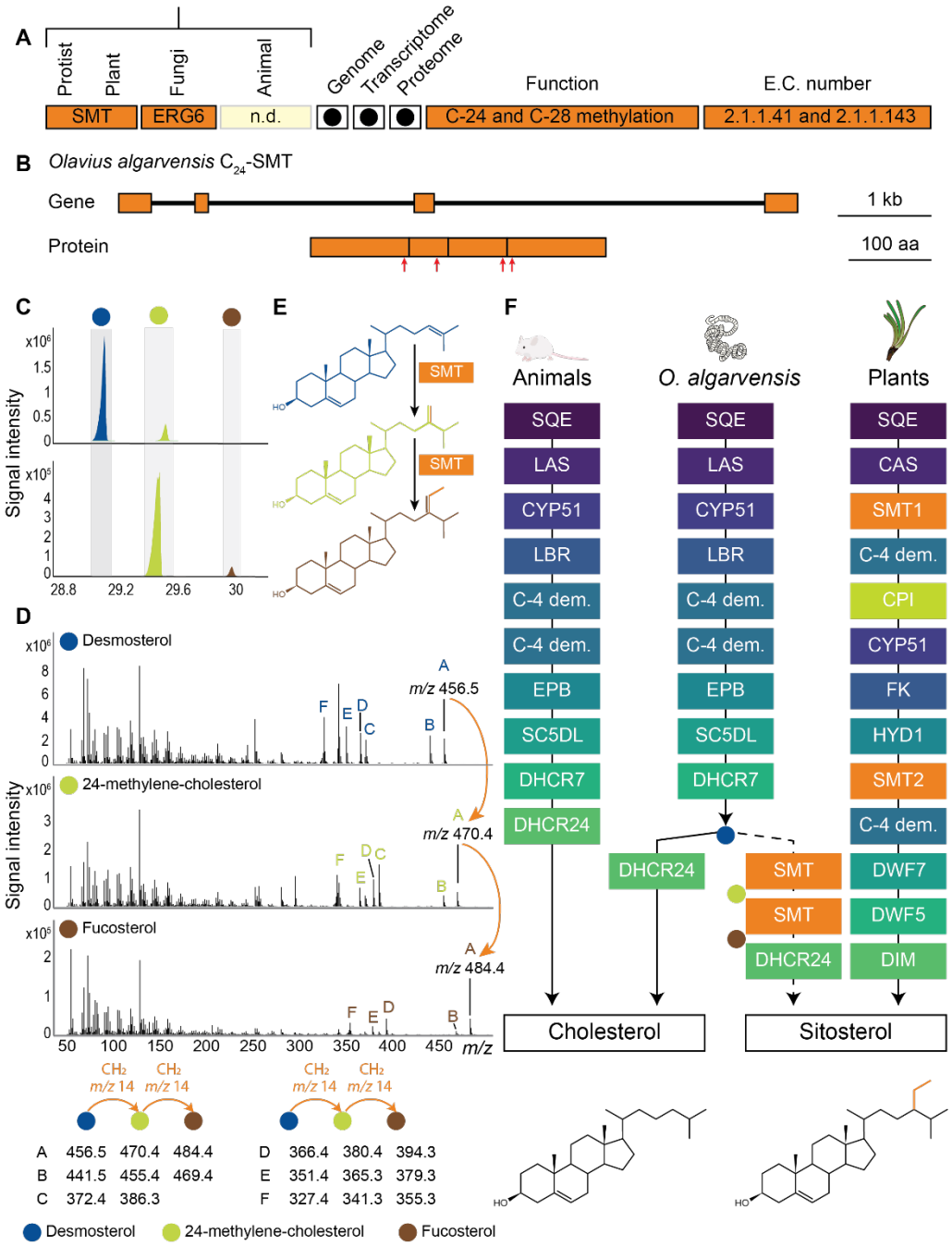

Figure 2 | *Olavius algarvensis* encodes and expresses a C_{24}-SMT which catalyzes two consecutive methylations, using desmosterol as the first and 24-methylene-cholesterol as the second substrate. A, *O. algarvensis* encodes and expresses a homolog of C_{24}-SMT, an enzyme not previously found in bilaterian animals and

essential to sitosterol synthesis. Dots indicate detection in the genome, transcriptome and proteome of *O. algarvensis*. **B,** The *O. algarvensis* C_{24}-SMT gene consists of 4 exons forming a 1071 bp open reading frame encoding a 356 amino-acid polypeptide. The four conserved regions of the enzyme are highlighted by red arrows. **C,** Chromatograms of enzymatic assays with desmosterol (top) and 24-methylene-cholesterol (bottom) as substrates**.** *O. algarvensis* C_{24}-SMT, after overexpression in *E. coli*, added a methyl group to the side chains of desmosterol and 24-methylene-cholesterol. In the first methylation desmosterol, an intermediate of cholesterol synthesis, was methylated to produce 24-methylene-cholesterol (C_{28} sterol). In the second methylation, 24-methylene-cholesterol was methylated to produce fucosterol (C_{29} sterol). **D,** Mass spectra of the different substrates and methylated products from the enzymatic assays. Sterol intermediates differ by the number of methyl groups (CH_2 at *m/z* 14) attached to their side chain. The side chain of desmosterol is not methylated, 24-methylene-cholesterol has a methyl group at C-24, and fucosterol has two methyl groups at C-24 and C-28**.** The substrates and methylated products were identified by MS, retention time and comparison with standards. The fragmentation pattern suggests that the methyl groups were added to the side chain of the sterols. **E,** Structural representation of the two methylation steps in *O. algarvensis*. **F,** Comparison of the enzyme used in the proposed sterol synthesis pathways in *Olavius* to the canonical cholesterol and sitosterol synthesis pathways (similar enzymatic reactions are colored similarly)**.** The first six steps are common to both cholesterol and sitosterol synthesis pathways. This trunk pathway branches off after the synthesis of desmosterol. For sitosterol synthesis, desmosterol is first methylated by C_{24}-SMT to 24-methylene-cholesterol, which is then methylated in a second, consecutive step by C_{24}-SMT to fucosterol. Fucosterol is reduced to sitosterol by a sterol C24-reductase (DHCR24, DIM). Squalene monooxygenase (SQE), oxydosqualene cyclase (LAS, CAS), sterol 14 demethylase (CYP51), sterol 14-reductase (LBR, FK), C-4 demethylation (C-4 dem.), Sterol Δ7-Δ8 isomerase (EBP, HYD1), sterol 5-desaturase (SC5DL, DWF7), sterol Δ7 reductase (DHCR7, DWF5), and C-24 sterol methyltransferase (C_{24}-SMT, SMT1, SMT2).

After confirming the first methylation step at C-24, we next searched for potential substrates for the second methylation step at C-28. This second methylation is essential as sitosterol is a C_{29} compound, characterized by the presence of two methyl groups on its side chain. To test our hypothesis that both of these methylations are catalyzed by the *O. algarvensis* C_{24}-SMT, we selected the product of the first methylation, 24-methylene-cholestrol, as well as campesterol, as potential substrates for the second methylation (**Supplementary Figure 20**). 24-methylene-cholesterol was the only substrate to which the *O. algarvensis* C_{24}-SMT added a methyl group, producing the C_{29} compound fucosterol (**Figure 2 and Supplementary Figure 20 and 21**). 24-methylene-cholesterol is the product of the methylation of desmosterol, providing evidence to support our hypothesis that in *O. algarvensis*, the C-24 and C-28 methylations are catalyzed by the same enzyme and occur consecutively. That is, the *O. algarvensis* C_{24}-SMT first methylates desmosterol at C-24 to produce the C_{28} sterol 24-methylene-cholesterol, and then adds a second methyl group to 24-methylene-cholesterol at C-28, to produce the C_{29} sterol fucosterol. Fucosterol differs from sitosterol by the presence of a double bond at position C-24(28). This double bond is most likely removed by the delta(24)-sterol reductase (DHCR24), which is expressed based on its presence in *O. algarvensis* transcriptomes (**Supplementary Figure 4 and 14**). These results provide

268 the first evidence for an animal C_{24}-SMT able to catalyze the two methylation steps
269 needed to synthesize sitosterol from a cholesterol intermediate, revealing a previously
270 unknown pathway for phytosterol synthesis in animals (**Figure 2**).

271 **C_{24}-SMT homologs are widespread in annelids**

272 Having demonstrated the activity of an animal C_{24}-SMT homolog that enables *O.*
273 *algarvensis* to synthesize sitosterol *de novo*, we asked if other gutless annelids also
274 encode functional C_{24}-SMTs. To answer this question, we analyzed the sterol contents
275 of six additional gutless annelid species, collected at locations in the Mediterranean Sea
276 (Elba, Mallorca, Monaco) and the Caribbean Sea (Bahamas, Belize). All six species had
277 similar lipid profiles as *O. algarvensis*, with sitosterol as their major sterol
278 (**Supplementary Table 6 and Supplementary information**).

279 In addition to lipid profiling, we screened the transcriptomes of nine *Olavius* and
280 *Inanidrilus* species and found all nine species expressed a C_{24}-SMT homolog
281 **(Supplementary Table 7)**, including *O. ilvae*, which had similarly negative sitosterol
282 $\delta^{13}C$ values as *O. algarvensis* (**Figure 1E**) and also encodes a C_{24}-SMT in its genome
283 (**Supplementary Table 3**). We confirmed the C-24 methylation ability of a second C_{24}-
284 SMT homolog, from *O. clavatus*, by heterologously expressing this gene in *E. coli*. Our
285 biochemical assays demonstrated that the C_{24}-SMT from *O. clavatus* is also a
286 bifunctional sterol methyltransferase, capable of methylating zymosterol, desmosterol
287 and 24-methylene-cholesterol (**Supplementary Figure 16, 17 and 21**).

288 We next asked if C_{24}-SMT homologs are present in other annelids. We screened
289 published transcriptomes and identified C_{24}-SMTs homologs in three deep-sea gutless
290 tubeworm species and in 17 gut-bearing annelid species from marine, limnic and
291 terrestrial environments (**Supplementary Table 8**). Despite the presence of C_{24}-SMT
292 homologs in these annelids, the published sterol profiles of annelids, including four gut-
293 bearing species analyzed in this study, are dominated by cholesterol (**Supplementary**
294 **Table 8, Figure 1A)**. However, sitosterol and other methylated/ethylated sterols (C_{28}
295 and C_{29} sterols) account for a considerable proportion of total sterols at 15-30% in some
296 of these species, including the hydrothermal vent and cold seep tubeworms *Riftia*

297 *pachyptila* and *Paraescarpia echinospica* (**Supplementary Table 8**). These deep-sea
298 siboglinid annelids are only distantly related to *Olavius* and *Inanidrilus*, but also lack a
299 gut and gain all of their nutrition from their chemosynthetic symbionts (Bright & Giere,
300 2005). The sterol contents of these tubeworms are dominated by cholesterol and
301 desmosterol, but the C_{28} sterol campesterol and other phytosterols make up as much as
302 nearly one third of their sterol contents (Guan et al., 2021; Phleger et al., 2005; Rieley et
303 al., 1995). Our discovery of C_{24}-SMTs homologs in these deep-sea annelids indicate
304 that these tubeworms are able to synthesize phytosterols as well.

305 **Bona fide C_{24}-SMT homologs are present in at least three animal phyla: sponges,**
306 **rotifers and annelids**

307 To assess the broader distribution of C_{24}-SMT homologs among animals, we performed
308 protein searches against public databases (see Materials and Methods for details). Hits
309 were found in six other animal phyla: sponges, cnidarians, mollusks, nematodes,
310 chordata and rotifers. Of these, the C_{24}-SMT homologs detected in sponges, rotifers
311 and annelids were identified as bona fide animal C_{24}-SMTs (**Figure 3, Supplementary**
312 **information**) and are described in the next paragraph. The C_{24}-SMTs recovered from
313 cnidarians, mollusks and chordata are unlikely to originate from the animals themselves.
314 Their phylogenetic placement and high similarities to plant, algal and protist sequences
315 suggest that these sequences originated from these animals' diets or are contaminants
316 (**Supplementary Figure 22 and Supplementary information**). We also found hits in
317 some nematodes, but these belonged to a group of C-4 sterol methyltransferases (C_4-
318 SMTs), that are specific to nematodes (Chitwood, 1991; Darnet et al., 2020) and
319 phylogenetically distinct from C_{24}-SMTs (**Figure 3B, Supplementary Figure 22**).

320

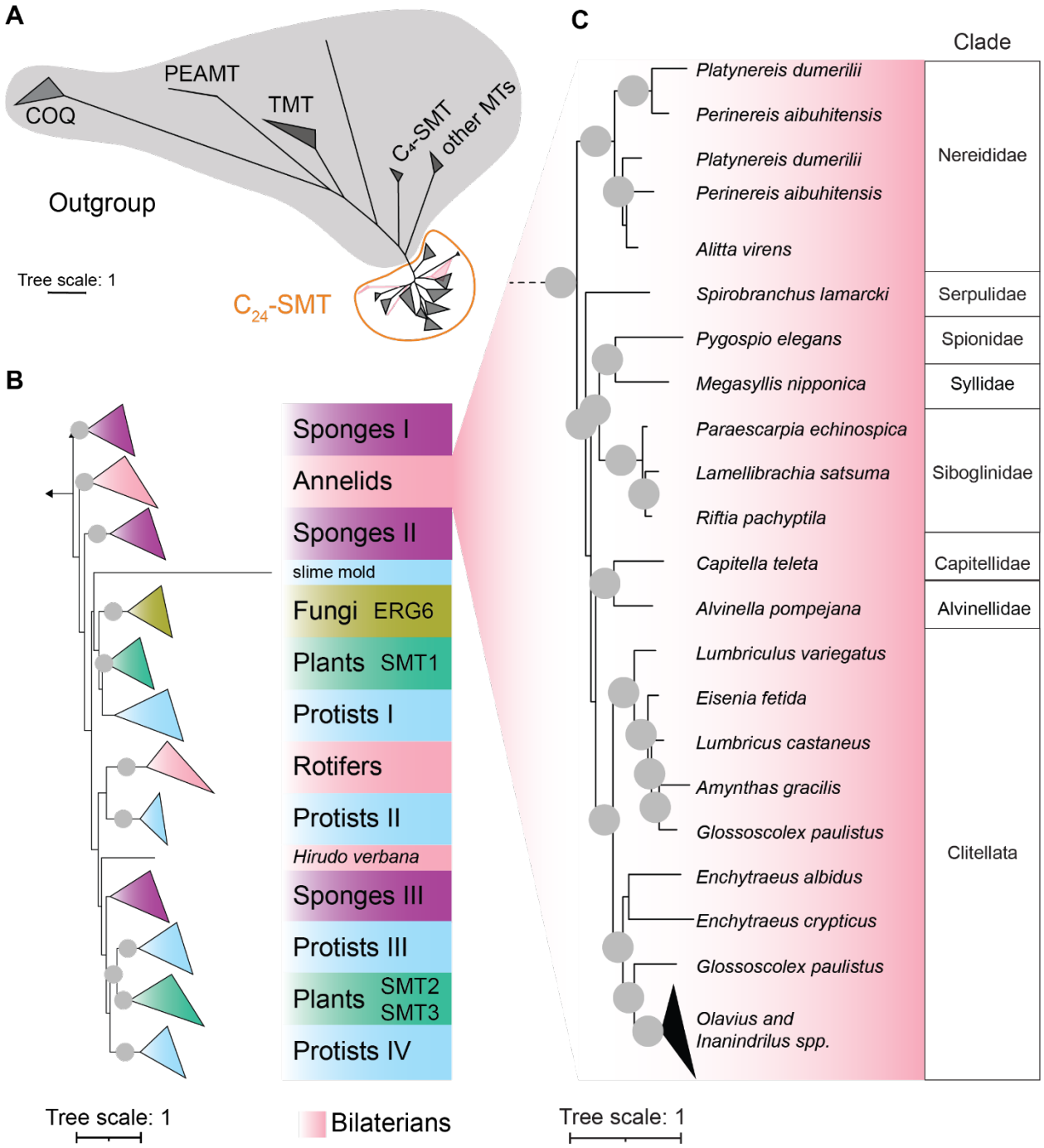

321

322 **Figure 3 | C_{24}-SMTs are widely distributed across animals, particularly sponges, rotifers and annelids.**
323 **A,** The animal C_{24}-SMT sequences cluster with bona fide plant and fungal C_{24}-SMTs and are phylogenetically distant
324 from other SAM-dependent methyltransferases (outgroup: Ubiquinone biosynthesis O-methyltransferase (COQ),
325 phosphoethanolamine N-methyltransferase (PEAMT), tocopherol O-methyltransferase (TMT), C_4 sterol
326 methyltransferase (C_4-SMT)). Unrooted maximum likelihood amino acid tree for eukaryotic SAM-dependent
327 methyltransferases. **B,** Maximum likelihood amino acid tree of eukaryotic C_{24}-SMTs. Sequences were clustered at
328 95% identity to make the tree more readable. Nodes with bootstrap value > 95 % are marked with grey circles. The

329 tree is rooted at midpoint. **C,** C_{24}-SMT homologs were detected in annelids from eight clades and were found in
330 marine, limnic and terrestrial species.

331 Our phylogenetic analyses of bona fide C_{24}-SMTs revealed that these fall into 12 clades
332 (**Figure 3**). These 12 clades include canonical C_{24}-SMTs from plants (SMT1 and
333 SMT2/SMT3) and fungi (ERG6), which have been extensively characterized in previous
334 studies (e.g. (Bouvier-Navé et al., 1998, p.; Haubrich et al., 2015; Nes et al., 2004)).
335 Animal C_{24}-SMTs do not cluster with these plant and fungi clades, suggesting that these
336 canonical C_{24}-SMTs were lost in the lineage leading to animals. Animal C_{24}-SMTs fell in
337 five subgroups. Three of these animal subgroups are from sponge C_{24}-SMTs and are
338 widely distributed across the tree. The remaining two animal clades contain sequences
339 from annelids and rotifers (**Supplementary Information**) The annelid clade includes
340 the C_{24}-SMTs we discovered in gutless *Olavius* and *Inanidrilus*, and have shown are
341 functional in producing sitosterol *de novo* in these animals. This clade also includes the
342 C_{24}-SMTs from all other annelids (26 species). These C_{24}-SMTs are widely distributed
343 across the annelid tree in eight orders, and in annelids from limnic, terrestrial and
344 marine environments (**Figure 3**). Given that the phylogeny of C_{24}-SMT corresponds well
345 to the phylogenetic evolution of annelids (**Figure 3**), it is likely that C_{24}-SMT was present
346 in the last common ancestor of annelids.

347 Conclusions

348 Here we describe and characterize a non-canonical animal C_{24}-SMT that enables
349 animals to synthesize sitosterol in a previously undescribed pathway that is distinct from
350 that of plants.

351 Our phylogenetic analyses of C_{24}-SMTs provide new insights into the evolutionary
352 history of sterols in eukaryotes. While ubiquitous in plants and fungi, C_{24}-SMTs were
353 thought to be largely absent from animals (Haubrich et al., 2015; Volkman, 2005). Prior
354 to this study, animal C_{24}-SMT sequences had only been reported in a few sponges (one
355 of the earliest diverging animal lineages) (Germer et al., 2017; Gold et al., 2016) and the
356 annelid *Capitella teleta* (Najle et al., 2016), but the activity of these enzymes remains
357 uncharacterized and their role in phytosterol synthesis was not explored. It has been

358 assumed that C_{24}-SMTs were present in the last eukaryotic common ancestor (LECA)
359 and then lost in the animal branch (Desmond & Gribaldo, 2009; Gold et al., 2016;
360 Haubrich et al., 2015). Our results, however, indicate that while the ancestral homologs
361 that led to extant plant and fungal C_{24}-SMTs were lost in the lineage leading to animals,
362 they retained non-canonical C_{24}-SMTs. These non-canonical C_{24}-SMTs are present in
363 at least three animal phyla, and sitosterol is the dominant sterol in at least some of
364 these animals, particularly *Olavius* and *Inanidrilus*. Our analyses also revealed that the
365 C_{24}-SMTs sequences isolated from sponges and protists are widely distributed across
366 the animal tree, suggesting that ancestral eukaryotes may have had several copies of
367 the C_{24}-SMT enzyme and flexible sterol synthesis pathways. While previous
368 phylogenetic analyses indicated that at least one copy of the C_{24}-SMT gene was
369 present in LECA (Desmond & Gribaldo, 2009; Gold et al., 2016), our data suggest that
370 more copies were present in the LECA and that the evolutionary history of sterol
371 synthesis pathways is more complex than previously assumed. Our results furthermore
372 challenge the widespread assumption that sterols can be used as geological biomarkers
373 for teasing apart the evolutionary history of early plants and animals (Summons et al.,
374 2022).

375 Given that C_{24}-SMTs are widespread in animals, how can we explain the unusually high
376 abundance of phytosterols in gutless *Olavius* and *Inanidrilus*? As described above,
377 other gutless animals that gain their nutrition from chemosynthetic symbionts (such as
378 vent and seep tubeworms) also have C_{28} and C_{29} sterol, but only *Olavius* and *Inanidrilus*
379 have higher amount of sitosterol than cholesterol. Sterols play many essential roles in
380 eukaryotes and their homeostasis is tightly regulated by complex mechanisms (Luo et
381 al., 2020; Wollam & Antebi, 2011). Animal membranes are usually dominated by
382 cholesterol, but studies have shown that phytosterols can be incorporated into animal
383 membranes (Mouritsen & Zuckermann, 2004) and can have beneficial effects on
384 animals. For example, they act as cholesterol-lowering agents, have anti-tumor, anti-
385 inflammatory, antibacterial and antifungal properties (Bin Sayeed & Ameen, 2015;
386 Saeidnia et al., 2014), and modulate interactions between bacterial pathogens and
387 eukaryotic hosts (van der Meer-Janssen et al., 2010). Therefore, the anti-inflammatory
388 and antibacterial properties of sitosterol, as well as its ability to protect animal cells

389 against toxins that target cholesterol (Li et al., 2015), might play a role in the symbiosis
390 between *Olavius* and *Inanidrilus* and their chemoautotrophic symbionts, by preventing
391 the symbionts from entering the host cytoplasm. In addition, changes in sterol
392 composition affect the fluidity and permeability of membranes, and these physical
393 changes in turn affect many cellular processes. For example, the high levels of
394 sitosterol in *Olavius* and *Inanidrilus* might increase the permeability of their membranes
395 for dissolved gases from their environment. These hosts compete with their aerobic
396 symbionts for the little oxygen available in their environment. Under oxic conditions,
397 these worms' symbionts consume 90% of the oxygen taken up by the worms (Häusler,
398 Lott and Dubilier, unpublished results), indicating that the worms may often experience
399 oxygen limitation. Furthermore, sitosterol has been shown to enhance mitochondrial
400 energy metabolism in a mouse cell line (Shi et al., 2013), and might enable *Olavius and*
401 *Inanidrilus* to gain more energy under low oxygen concentrations in their environment.
402 While additional studies are needed to elucidate the physiological and/or ecological
403 roles of sitosterol in animals, *Olavius and Inanidrilus* are valuable model systems for
404 studying the impact of phytosterols on animal membrane properties *in vivo* and
405 furthering our understanding of the roles sterols play in eukaryotic cells.

406 Materials and Methods

407 **Reagents.** All organic solvents were LC–MS grade: acetonitrile (ACN; Honeywell,
408 Honeywell Specialty Chemicals), chloroform (Merck), isopropanol (IPA; BioSolve),
409 methanol (MeOH; BioSolve), hexane (Sigma-Aldrich), acetone (Sigma-Aldrich), ethanol
410 (EtOH; Sigma-Aldrich) and formic acid (FA; Sigma-Aldrich). Water was deionized using
411 the Astacus MembraPure system (MembraPure). Pyridine (dried (max. 0.0075% H_2O)
412 SeccoSolv®) was obtained from Sigma-Aldrich. The reagents used for GC-MS
413 derivatization were obtain from Chromatographie Service and Sigma-Aldrich. The
414 internal standards (5α-cholestane and Ribitol) used for GC-MS analysis were obtained
415 from Sigma-Aldrich.

Sampling

Gutless annelids. Sediments in which gutless annelids occur were collected by scuba diving. The worms were extracted manually from the sediment and either directly fixed in MeOH or kept in aquaria with seagrass and sediment from the collection site for up to one year before use in experiments. Six gutless annelid species, belonging to two different genera were collected in five locations: the bay of Sant'Andrea (Island of Elba, Italy) (42° 48'29.4588" N; 10° 8' 34.4436" E), the bay of Magaluf (Mallorca, Spain) (39º 30' 14.814'' N; 2º 32' 35.868'' E), at Carrie Bow Cay (Belize) (16° 04' 59" N; 88° 04' 55" W), Twin Cayes (Belize) (16° 50' 3" N; 88° 6' 23" W), and Okinawa (Japan) (26° 29' 33.4" N; 127° 50' 31.6" E).

Gut-bearing annelids. *Cirratulidae sp.*, *Heronidrilus sp.* and *Rhyacodrilus sp.* were collected in Belize in the same environments as the gutless annelids. They were extracted manually from the sediment and directly fixed in MeOH. *Tubifex tubifex* specimens were purchased in an aquarium shop and kept in aquaria for two weeks before fixation in MeOH. *Capitella teleta* worms were provided by the Meyer Lab (https://wordpress.clarku.edu/nmeyer/) and kept in aquarium before fixation in MeOH. The MeOH fixed samples were stored at - 20°C until extraction.

Seagrass. Seagrass plants (*Posidonia oceanica*) were collected by scuba diving in the bay of Sant'Andrea (Elba, Italy) (42° 48' 29.4588" N; 10° 8' 34.4436" E). The leaves, roots and rhizomes were dissected using a razor blade, placed into individual bags and stored at -20°C.

Porewater. Porewater was collected from sediments for metabolomic analyses. We sampled in and near seagrass meadows in the Mediterranean Sea in the bay of Sant'Andrea (Elba, Italy) (42° 48' 29.4588" N; 10° 8' 34.4436" E) and in the Caribbean at Carrie Bow Cay (Belize) (16° 04' 59" N; 88° 04' 55" W) and Twin Cayes (Belize) (16° 50' 3" N; 88° 6' 23" W). Using a steel lance (1 m long, 2 mm inner diameter) fitted with a wire mesh (63 µm) to prevent the intake of sediment and seagrass, porewater was slowly extracted from sediments into polypropylene syringes. A porewater profile

444 consisted of top to bottom sampling of the sediments every 5 or 10 cm down to 30 cm.
445 For metabolomic analysis, 10 mL samples were stored at -20°C until further processing.

446 Metabolite extraction

447 **Gutless and gut-bearing annelids.** Metabolites were extracted from the worms using
448 the following method for metabolite profiling: Tissues from MeOH fixed worms were
449 transferred to 2 mL screwcap tubes containing a mix of silica beads (Sigmund Linder).
450 The residual methanol was added to the screw cap tube. The tubes were spiked with
451 100 µL 5α-cholestane (1 mM) and 40 µL ribitol (0.2 mg mL^{-1}). 0.5 mL pre-cooled
452 extraction solution (ACN:MeOH:water (v:v:v) 2:2:1) was added to each tube.

453 Tissues were disrupted by bead beating for 2 cycles of 40 sec (4 m sec^{-1}). The tissues
454 were pelleted by centrifugation (9,600 x g, 2 min), and the supernatants transferred to
455 new tubes. The pellets were extracted one more time with 1.5 mL of extraction solution.
456 The supernatants were combined and evaporated to dryness in a vacuum concentrator
457 without heating (approximately 1.5 h). The obtained aliquots were stored at -20°C until
458 metabolite derivatization.

459 **Seagrass.** The frozen plant tissues were ground to a fine powder in liquid nitrogen
460 using a pestle and mortar. 70 mg of the powder was transferred to 2 mL screw cap
461 tubes containing 1.2 mL MeOH (pre-cooled at -20°C). The tubes were vortexed for 10 s.
462 The internal standards were added to the tubes: 40 µL ribitol (0.2 mg mL^{-1}) and 100 µL
463 5α-cholestane (1 mM), and the tubes were vortexed for another 10 sec. The tubes were
464 placed on a thermomixer and shaken for 10 min at 70°C at 950 rpm. The plant powder
465 was pelleted by centrifugation (10 min, 11,000 × g, 4°C). The supernatant was
466 transferred into a new 2 mL Eppendorf tube and evaporated to dryness using a
467 Concentrator Plus (Eppendorf) (V-AL, 1.5 h, 45°C). The dried extracts were stored at -
468 20°C until metabolite derivatization.

469 **Porewater.** Sterols were extracted using Superclean LC-18 SPE tubes (6 mL, 0.5 g,
470 Supelco). The silica cartridge was equilibrated using an ultra-pure water (UPW):MeOH
471 dilution series (0:1, 1:4, 1:1, 4:1, 1:0 [v/v]). The porewater samples were spiked with

472 internal standard (100 µL 5α-cholestane (1mM)), before being loaded on the column.
473 Impurities were removed by three successive UPW washes, and the sterols eluted from
474 the cartridge with 3 × 5 mL of MeOH. The MeOH fractions were collected and
475 evaporated to dryness using a Concentrator Plus on V-AL mode with centrifugation at
476 30°C. Positive and negative controls were run in parallel. For negative controls sterols
477 were extracted from 10 mL of artificial sea water (ASW). As with positive controls, 10
478 mL ASW was spiked with 20, 40, or 80 nmol cholesterol and β-sitosterol. The dried
479 extracts were stored at -20°C until metabolite derivatization.

480 GC-MS analysis

481 **Derivatization.** To remove condensation formed during storage, we further dried the
482 extracts in a vacuum concentrator for 30 min prior to sample preparation for GC-MS
483 analysis.

484 **Gutless and gut-bearing annelids.** Metabolite derivatization was performed by adding
485 80 µL methoxyamine hydrochloride (MeOX) dissolved in pyridine (20 mg mL^{-1}) to the
486 dried pellet and incubating for 90 min at 37°C using a thermomixer (BioShake iQ,
487 Analytik Jena) under constant rotation at 1350 rpm. Following the addition of 100 µL
488 N,O-Bis(trimethylsilyl)trifluoroacetamide (BSTFA), each extract was vortexed, and
489 incubated for another 30 min at 37°C on a thermomixer under constant rotation at 1350
490 rpm. After a short centrifugation, 100 µL of the supernatant was transferred to a GC-MS
491 vial (Insert G27, sping S27 and Mikor-KH-Vial G1; Chromatographic Service) for GC-
492 MS data acquisition.

493 **Seagrass.** 80 µL of MeOX (20 mg mL^{-1} dissolved in pyridine) was added to the dried
494 extracts. The resuspended dried extracts were vortexed for a few seconds and placed
495 on a thermomixer (BioShake iQ, Analytik Jena) for 90 min (37°C, 1200 rpm). 80 µL
496 BSTFA was added to the tubes. The tubes were vortexed for a few seconds and placed
497 on a thermomixer for 15 min (60°C, 1200 rpm). After a short centrifugation, 100 µL of
498 the supernatant was transferred into GC-MS vials (Insert G27, sping S27 and Mikor-KH-
499 Vial G1; Chromatographic Service) and analyzed by GC-MS.

500 **Porewater.** After complete evaporation, 80 µL BSTFA was added to the tubes. The
501 tubes were gently vortexed and placed on a thermomixer for 15 min (60°C, 950 rpm).
502 After a short centrifugation (1 min, 7,800 x g), the supernatant was transferred into GC-
503 MS vials and analyzed.

504 **Data acquisition.** The analysis of all metabolomic samples was conducted on a 7890B
505 GC system (Agilent Technologies) coupled to a 5977A single quadrupole mass
506 selective detector (Agilent Technologies). The gas chromatograph was equipped with a
507 DB-5 ms column (30 m × 0.25 mm, film thickness 0.25 µm; including 10 m DuraGuard
508 column, Agilent Technologies) and a GC inlet liner (ultra inert, splitless, single taper,
509 glass wool, Agilent). Helium was used as gas carrier at a constant flow (0.8 mL min^{-1}).
510 An Agilent 7693 autosampler injected 1 µL of derivatized sample in splitless mode. The
511 injector temperature was set at 290°C. The temperature program started at 60°C for 2
512 min, then increased to 300°C at 10°C min^{-1}, and held at 325°C for 7 min. Mass spectra
513 were acquired in electron ionization mode at 70 eV across the mass range of 50–600
514 *m/z* and a scan rate of 2 scans sec^{-1}. The retention time was locked using a standard
515 mixture of fatty acid methyl esters (Sigma-Aldrich).

516 **Data analysis.** Sterols were identified through comparison with standards using the
517 Mass Hunter Suite (Agilent) and through comparison to the NIST database. Sterols
518 were further quantified using the Mass Hunter Quantification Suite (Agilent).

519 HPLC-MS

520 **High-resolution LC–MS/MS.** The analysis was performed using a QExactive Plus
521 Orbitrap (Thermo Fisher Scientific) equipped with a HESI probe and a Vanquish
522 Horizon UHPLC system (Thermo Fisher Scientific). The lipids were separated on an
523 Accucore C30 column (150 × 2.1 mm, 2.6 µm, Thermo Fisher Scientific), at 40°C, using
524 a solvent gradient. Buffer A (60:40 ACN:H2O, 10 mM ammonium formate, 0.1% FA)
525 and buffer B (90:10 IPA:ACN, 10 mM ammonium formate, 0.1% FA) (Breitkopf et al.,
526 2017) were used at a flow rate of 350 µl min^{-1}. The lipids were eluted from the column
527 with a gradient starting at 0% buffer B (**Supplementary Table 10**). The injection volume

528 was 10 µl. In the same run, MS measurements were acquired in positive-ion and
529 negative-ion mode for a mass detection range of *m/z* = 150–1,500. Resolution of the
530 mass analyzer was set to 70,000 for MS scans and 35,000 for MS/MS scans at *m/z* =
531 200. MS/MS scans of the eight most abundant precursor ions were acquired in positive-
532 ion and negative-ion modes. Dynamic exclusion was enabled for 30 sec and collision
533 energy was set to 30 eV (for more details see **Supplementary Table 11**). The data
534 were analyzed with Thermo FreeStyle™ (version 1.6) and Xcalibur Quan Browser
535 Software v. 2.0.3 (Thermo).

536 GC-IRMS

537 **Sample preparation**. Sterols were extracted from the gutless annelids *O. algarvensis*
538 and *O. ilvae*, as well as from the rhizome and leaves of *P. oceanica*. All samples were
539 extracted with dichloromethane:MeOH (2:1) three times. The resulting total lipid extracts
540 were then separated by solid phase extraction with a Machery & Nagel aminopropyl
541 modified silica gel column (500mg) into four fractions with increasing polarity (see
542 (Birgel et al., 2008)). For the sterols, the third fraction was used
543 (dichloromethane:acetone 9:1). Prior to measurement on the GC-MS and GC-IRMS, the
544 samples were silylated with BSTFA. The porewater samples were extracted as
545 described above.

546 **Data acquisition.** The resulting sterols were identified on a Thermo Electron Trace
547 DSQ II coupled gas chromatograph mass spectrometer (GC-MS). The GC-MS was
548 equipped with a 30 m HP-5 MS UI fused silica capillary column (0.25 mm diameter, 0.25
549 µm film thickness). The carrier gas was helium. The GC temperature program was as
550 follows: 60°C (1 min), from 60°C to 150°C at 10°C min^{-1}, from 150°C to 325°C at 4°C
551 min^{-1}, 25 min isothermal. Identification of compounds was based on retention times and
552 published mass spectral data. Compound-specific carbon stable isotope compositions
553 of sterols were measured on a gas chromatograph (Agilent 6890) coupled with a
554 Thermo Finnigan Combustion III interface to a Finnigan Delta Plus XL isotope ratio
555 mass spectrometer (GC-IRMS). The GC conditions were identical to those described
556 above for GC-MS analyses. All sterols were corrected for the additional carbons

557 introduced by derivatization with BSTFA. The standard deviation of the isotope
558 measurements was < 0.8‰.

559 MALDI-2-MSI

560 **Sample preparation.** The worms were prepared following Kadesch et al. (2019) with a
561 few modifications. Briefly, 20 µL 6.7% glutaraldehyde solution in marine phosphate
562 buffered saline were deposited on a glass slide. Gutless annelids were transferred to
563 the fixative using bent acupuncture needles. A coverslip was applied, and samples were
564 frozen in liquid nitrogen and stored at −80°C until further processing.

565 A single worm was transferred using featherweight forceps onto a sodium
566 carboxymethyl cellulose (CMC; Sigma-Aldrich) stamp which was glued onto a cryostat
567 specimen disc (Leica). Gelatin solution (8 % (β = 80 g L^{-1}), 10-20 µL) was used to coat
568 the worm. The specimen disc with the sample was transferred to the cryostat (Leica
569 CM3050 S, Leica Biosystems) and kept for 30 min at -22°C before sectioning into
570 sections of 12 µm thickness (chamber temperature -22°C, object temperature -22°C).
571 Sections were thaw-mounted on IntelliSlides (Bruker Daltonics), and their quality
572 determined microscopically. Sections of sufficient quality were stored in a desiccator at
573 room temperature (RT) until further analysis.

574 **Matrix application and data acquisition.** The matrix 2′,5′-dihydroxyacetophenone
575 (DHAP; Merck) was applied by sublimation and the data were acquired on a modified
576 timsTOF fleX instrument (Bruker Daltonics, Bremen, Germany) (Soltwisch et al., 2020)
577 as described in (Bien et al., 2021). The mass resolving power of this hybrid QTOF-type
578 instrument is about 40,000 (fwhm) in the investigated *m/z* range of 300–1500. For
579 material ejection, a scan range of 1 µm of the laser spot on the target was used,
580 resulting in an ablated area of 5 µm in diameter. The step size of the stage during the
581 MSI run was set to 5 µm. The laser power was set to 40%, with 50 laser shots/pixel.

582 **Data analysis.** SCiLS lab (Bruker Daltonics, version 2021a) was used for data analysis
583 and to produce the ion images shown in the figures. For image visualization, an interval

584 width of 15 ppm was used. The ion images represent the data after root mean square
585 normalization and without denoising.

586 TOF-SIMS

587 **Sample preparation.** *O. algarvensis* specimens were fixed with 4% paraformaldehyde
588 (PFA) at 4°C for 4 h. The fixative was removed by washing three times with marine
589 phosphate buffer. The washed samples were then stored at -20°C in MeOH.

590 PFA-fixed samples were embedded in paraffin. The MeOH was exchanged with pure
591 EtOH by three successive incubations of 60 min in pure EtOH at RT. The samples were
592 then incubated in RothiHistol (30 min, 60 min, and overnight at RT). The samples were
593 then infiltrated with paraffin at 60°C, they were placed in fresh paraffin three times for
594 30, 60 and 60 min and then left to incubate overnight. For embedding, two-thirds of the
595 embedding mold was filled with paraffin. The sample was placed in the mold and the
596 mold was filled completely with paraffin. The sample was aligned and left to polymerize
597 for one week. After polymerization, a microtome was used to cut 4 µm sections. The
598 sections were placed on poly-L-lysine-coated glass slides (Sigma-Aldrich), left to air dry
599 overnight and baked at 60°C for 2 h to improve adherence to the slide. Finally, the
600 sections were de-waxed, first in three baths of 10 min in RothiHistol, followed by an
601 EtOH series (96%, 80%, 70%, 50%), and the slides were dipped in ultra-pure water and
602 left to air dry. Once dried they were wrapped in aluminum foil and stored in a desiccator
603 (Roth, Desiccator ROTILABO® Glass, DN 250, 8.0 l) until TOF-SIMS analysis.

604 **Data acquisition and analysis:** SIMS data were acquired on an IONTOF TOF-SIMS 5
605 instrument (IONTOF GmbH) using a 25 keV Bi_3^+ LMIG analytical beam in positive
606 mode. To obtain high-resolution mass spectra, high current bunch mode was used with
607 a beam current of ~1 pA. The analytical area was typically 100 μm^2. Secondary ion
608 maps were collected using the Bi_3^+ LMIG in burst alignment mode for greater lateral
609 resolving power (raster size: 512 x 512, FoV 210 x 210). The samples were also sputter
610 pre-cleaned using a 5 keV Ar_{1000}^+ cluster ion beam. The data were analyzed in
611 SurfaceLab 7 (IONTOF). We analyzed standards to determine the most abundant ions

612 produced by each sterol: cholesterol ($[M-H_2O+H]^+$ $C_{27}H_{45}$, at *m/z* 369.38; $[M-H]^-$
613 $C_{27}H_{45}O$, at *m/z* 385.34; $[M-H+O]^-$ $C_{27}H_{45}O_2$, at *m/z* 401.35) and sitosterol ($[M-H_2O+H]^+$
614 $C_{29}H_{49}$, at *m/z* 397.47; $[M-CH_3O]^-$ $C_{28}H_{47}$, at *m/z* 383.37; $[M-H]^-$ $C_{29}H_{49}O$, at *m/z* 413.45).
615 To determine the distribution of each sterol in *O. algarvensis* sections, the intensity of
616 the three most abundant ions was combined.

617 Sterol identification

618 Sterols were identified by comparison to chemical standards and MS database. Matching
619 mass spectra and retention time with sterol standards confirmed sterol identification. In
620 addition, tandem mass spectra were acquired with high-mass resolution and accuracy on
621 all sterols. Each sterol was identified on using a combination of two different
622 chromatography types (GC-MS and LC-MS), including different ionization methods
623 (electrospray ionization, electron impact ionization). For sterol identification with MSI we
624 used chemical standards for sterols and measured them with MALDI-2 and SIMS in
625 parallel to the tissue sections

626 Identification of genes involved in sterol biosynthesis in *O. algarvensis* 627 transcriptomes

628 Transcriptomes generated in a previous study (Wippler et al., 2016) were analyzed for
629 genes involved in sterol biosynthesis Protein sequences from humans, *Arabidopsis*
630 *thaliana* and *Saccharomyces cerevisiae* were used as queries (**Supplementary Table**
631 **12**) to search the transcriptomic assemblies with TBLASTN (e-value 1e-10). The identity
632 of the hits was confirmed by BLASTP search against the NCBI nr and Swiss-Prot
633 database as well as by INTERPROSCAN domain prediction. *O. algarvensis* sequences
634 were aligned with reference sequences (Desmond & Gribaldo, 2009) using Clustalw
635 (Larkin et al., 2007), trimmed with trimAl (Capella-Gutiérrez et al., 2009). Alignments
636 were used to calculate maximum-likelihood trees with ultrafast bootstrap support values
637 using IQ-TREE (Minh et al., 2020). The resulting trees were visualized using iTOL
638 (Letunic & Bork, 2019). The trees are shown in **Figure 3** and **Supplementary Figures**
639 **5** to **14.**

640 ## Gutless annelid nucleic acid extraction, sequencing and analysis

641 **Extraction and sequencing.** Genomic DNA was extracted from fresh specimens of two
642 gutless annelid species (*O. algarvensis* and *O. ilvae*, one individual each). High
643 molecular weight genomic DNA was isolated with the MagAttract HMW DNA Kit
644 (Qiagen). Quality was assessed by the Agilent FEMTOpulse and DNA quantified by the
645 Quantus dsDNA kit (Promega). DNA was processed to obtain a PacBio Sequencing-
646 compatible library following the recommendations outlined in "Procedure & Checklist –
647 Preparing HiFi Libraries from Low DNA Input Using SMRTbell Express Template Prep
648 Kit 2.0". Libraries were sequenced on a Sequel II instrument at the Max-Planck
649 Genome-Centre Cologne (MP-GC) with sequencing chemistry 2.0, binding kit 2.0 on
650 one 8M SMRT cell for 30 h applying continuous long read (CLR) sequencing mode.

651 **Assembly and identification of genes involved in sterol biosynthesis.** The CLR
652 reads were assembled using Flye (v 2.8) (Kolmogorov et al., 2019). The completeness
653 of the assembly was assessed with QUAST (v. 5.0.0) (Gurevich et al., 2013) and
654 BUSCO (version 5.2.2) (Seppey et al., 2019). *O. algarvensis* and *O. ilvae* sequences
655 were retrieved from the PacBio assembly with BLAT (Kent, 2002) and SCIPIO (version
656 1.4) (Keller et al., 2008) using *O. algarvensis* transcripts as queries.

657 ## Metaproteomics

658 **Protein identification and quantification.** We re-analyzed data produced by Jensen
659 (Jensen et al., 2021) using a customized database containing 1,439,433 protein
660 sequences including host and symbiont proteins as well as a cRAP protein sequence
661 database (http://www.thegpm.org/crap/) of common laboratory contaminants. We
662 performed searches of the MS/MS spectra against this database with the Sequest HT
663 node in Proteome Discoverer version 2.3.0.523 (Thermo Fisher Scientific). The
664 following parameters were used: trypsin (full), maximum two missed cleavages, 10 ppm
665 precursor mass tolerance, 0.1 Da fragment mass tolerance and maximum of 3 equal
666 dynamic modifications per peptide, namely: oxidation on M (+ 15.995 Da),
667 carbamidomethyl on C (+ 57.021 Da) and acetyl on the protein N terminus (+ 42.011

668 Da). False discovery rates (FDRs) for peptide spectral matches (PSMs) were calculated
669 and filtered using the Percolator Node in Proteome Discoverer (Spivak et al., 2009).
670 Percolator was run with a maximum delta Cn 0.05, a strict target FDR of 0.01, a relaxed
671 target FDR of 0.05 and validation based on q-value. We used the Protein FDR Validator
672 Node in Proteome Discoverer to calculate q-values for inferred proteins based on the
673 results from a search against a target-decoy database. Proteins with a q-value <0.01
674 were categorized as high-confidence identifications and proteins with a q-value of 0.01–
675 0.05 were categorized as medium-confidence identifications. We combined search
676 results for all samples into a multi-consensus report in Proteome Discoverer and only
677 proteins identified with medium or high confidence were retained, resulting in an overall
678 protein-level FDR of 5%.

679 C_{24}-SMT distribution in animals

680 **Gutless annelid search.** Total RNA was extracted from nine gutless annelid species.
681 RNA was quality and quantity assessed by capillary electrophoresis (Agilent
682 Bioanalyser PicoChip) and Illumina-compatible libraries were generated with the
683 NEBNext® Single Cell/Low Input RNA Library Prep Kit for Illumina®. Libraries were
684 again quality and quantity controlled followed by sequencing on a HiSeq 3000 device
685 with 2 × 150 bp paired-end read mode. The raw reads were trimmed and corrected, the
686 symbiont reads were mapped out and the host read assembled using Trinity. The
687 resulting assemblies were screened for C_{24}-SMT homologs using the model C_{24}-SMTs
688 (P25087, Q9LM02, Q39227) as subject. Only hits with e-values smaller than 1e-30 and
689 spanning at least half the subject sequences were kept for further analysis. The contigs
690 of interest were isolated and TransDecoder (v 5.5.0) (https://github.com/TransDecoder)
691 was used to identified candidate coding region TransDecoder, homology searches
692 (blastp and PFAM search) were used as additional retention criteria.

693 **Search in public databases.** To assess the presence of C_{24}-SMT homologs in other
694 animals, protein searches against NCBI (National Center for Biotechnology Information
695 (NCBI), available from: https://www.ncbi.nlm.nih.gov/) databases (nr, tsa_nr,
696 refseq_prot, env_nr and tsa) as well as the proteomes predicted by Ensembl metazoan

697 (Howe et al., 2020) and Compagen (Hemmrich & Bosch, 2008) were performed. The
698 search was restricted to metazoan sequences to avoid hits from fungi and viridiplantae.
699 Only hits with e-values smaller than 1e-30 and a coverage > 60% were retained for
700 further analysis.

701 **Phylogenetic tree.** A phylogenetic tree was constructed from selected C_{24}-SMT protein
702 sequences. Briefly, published C_{24}-SMT sequences (Desmond & Gribaldo, 2009; Gold
703 et al., 2016) were downloaded from UniProt and JGI Genome Portal and used as
704 references. Other SAM-dependent methyltransferases (ubiquinone biosynthesis O-
705 methyltransferase, phosphoethanolamine N-methyltransferase, tocopherol O-
706 methyltransferase and C_4-sterol methyltransferase) were used as outgroups. Together
707 with the animal C_{24}-SMTs these sequences were clustered (95% ID), aligned using
708 Clustalw 2.1 (Larkin et al., 2007) and trimmed with TrimAl v1.2 (Capella-Gutiérrez et al.,
709 2009). IQ-TREE (v1.6.12) (Minh et al., 2020) was used to predict the best-fit models of
710 evolution and to calculate a maximum-likelihood tree with ultrafast bootstrap support
711 values from the concatenated alignment. The resulting tree was visualized using iTOL
712 v6 (Letunic & Bork, 2019).

713 C_{24}-SMT heterologous gene expression and enzyme assay

714 **Heterologous gene expression.** To determine the activity of the putative C_{24}-SMT
715 enzymes, we overexpressed OalgSMT, OclaSMT and ArathSMT1 (**Supplementary**
716 **Table 13**) in *E. coli* and performed enzymatic assays. GenScript (Genscript®)
717 generated pet28a(+) (NheI/XhoI) plasmid containing the sequence of interest. For
718 expression, the pet28(a)-OalgSMT and pet28(a)-OclaSMT vectors were transformed in
719 Lemo21(DE3) *E. coli* competent cells (New England Biolabs (NEB)). The pet28(a)-
720 ArathSMT1 vector was transformed in Overexpress C43(DE3) pLysS *E. coli* competent
721 cells (Lucigen). A single colony of transformed cells was grown in 3 mL lysogeny broth
722 (LB) supplemented with the appropriate antibiotics for 8 h (37°C, 150 rpm). 1 mL pre-
723 culture was used to inoculate 1 L ZYP-5052-Rich-Autoinduction-Medium (Studier, 2005)
724 supplemented with antibiotics and 1500 µM rhamnose. The cultures were grown for 72
725 h at 20°C, with rotation at 150 rpm. Cells were harvested by centrifugation at 4,500 × g

726 for 25 min at 4°C, the supernatant discarded and the resulting pellet stored at -20°C
727 until further use.

728 **Protein extraction/cell lysis.** The frozen pellets were thawed on ice. They were then
729 resuspended in 15 mL sucrose solution (750 mM sucrose solution in 20 mM phosphate
730 buffer at pH 7.5). Once the pellets were dissolved in the sucrose solution, 5 mg
731 lysozyme was added and the tubes shaken for 10 min at RT. Cells were lysed by
732 addition of 30 mL lysis buffer (100 mM NaCl, 15% glycerol, 3 mM EDTA in 20 mM
733 phosphate buffer at pH 7.5), 0.2 mL $MgSO_4$ stock solution (120 g L^{-1}) and 0.3 mL Triton
734 X-100. The mix was vigorously shaken and incubated on ice until it reached a
735 gelatinous consistency. The DNA was fragmented by addition of 2 mL DNase stock
736 solution (50 mg DNase I in 35 mL buffer (20 mM Tris-HCl pH8, 0.5 M NaCl) and 15 mL
737 glycerol). Finally, the cell fragments and inclusion bodies were pelleted by centrifugation
738 (45min, 16,000 × g, 4°C). The supernatant, containing soluble proteins, was aliquoted
739 and stored at -80°C until further use. The overexpression yielded a target protein
740 migrating on SDS-PAGE with the expected size of ~40 kDa.

741 **Enzymatic assay.** We tested nine sterol substrates (cycloartenol, lanosterol,
742 zymosterol, lathosterol, 7-dehydrocholesterol, desmosterol, campesterol, cholesterol
743 and 24-methylene-cholesterol) (**Supplementary Table 14**). The assay was performed
744 in 600 µL total volume. 100 µL crude soluble protein extract was mixed with 400 µL
745 phosphate buffer (20 mM, 5% glycerol, pH 7.5) in a 15 mL tube containing a sterol
746 substrate (final concentration 100 µM) dispersed in Tween 80 (0.1% v/v). The reaction
747 was initiated with 100 µL SAM working solution (0.6 mM). The reaction was performed
748 in a water bath at 35°C for 16 h. The reaction was terminated with 600 µL 10%
749 methanolic KOH. The products were extracted three times with 2.5 mL hexane and
750 mixed on a vortex for 30 s. The resulting organic layer was evaporated to dryness in a
751 concentrator at 30°C, V-AL for 1.5 h. Two internal standards, 5α-cholestane (100 µL, 1
752 mM solution) and ribitol (40 µL 200 mg/L solution), were added to the tubes and
753 evaporated to dryness. The samples were derivatized and analyzed on an Agilent GC-
754 MS as described above or directly analyzed on a QExactive Plus Orbitrap (Thermo
755 Fisher Scientific) equipped with a HESI probe and a Vanquish Horizon UHPLC system

(Thermo Fisher Scientific). The sterols were separated on a C18 column (Accucore Vanquish C18+, 100 x 2.1, 1.5 µm, Thermo Fischer Scientific), for method details see **Supplementary Table 11 and 15**.

Data availability

The metaproteomic mass spectrometry data have been deposited at the ProteomeXchange Consortium via the PRIDE partner repository (Vizcaíno et al., 2016) with the following dataset identifiers: PXD014881.

The upload of metabolomics and sequencing data on public platforms is in progress.

Author Contributions

D.M., M.L. and N.D. conceived the study. D.M. collected, processed and analyzed the metabolomic, metatranscriptomic and metagenomic data. T.B. and S.F. collected mass spectrometry imaging data. D.B. performed the GC-IRMS measurements. M.J. and M.K. collected and analyzed the proteomics data. C.Z. and D.M. performed the heterologous gene expression. D.M. performed the enzyme assay and analyzed the data. D.M. and M.L. wrote the manuscript together with N.D. and contributions from T.B., D.B., M.K., and C.Z..

Acknowledgments

We thank Alfred Garsdal, Janine Beckmann, Marvin Weinhold, Martina Meyer, Silke Wetzel, Tomasz Markowski, Tora Gulstad, Kristopher Caspersen and Frantisek Fojt from the Max Planck Institute for Marine Microbiology (MPI-MM) for support with data acquisition and sample preparation. We thank Miriam Sadowski and Grace D'Angelo for proof reading the manuscript. We are grateful to Alexander Gruhl, Yui Sato, Niko Leisch, Anna Mankowski, Silvia Bulgheresi, Claudia Bergin, Emilia M. Sogin and Katherine Schimdt for sample collections and help in the field. We thank the Meyer Lab for providing us with *Capitella teleta* worms. We also thank Bruno Huettel (Max Planck Genome Center, Cologne) for his support with sequencing. LC-MS/MS based proteomics measurements were made in the Molecular Education, Technology, and Research Innovation Center (METRIC) at North Carolina State University. We thank Bruker Daltonics for providing access to the prototype timsTOF flex MALDI-2 instrument and Jen Soltwisch and Klaus Dreisewerd for their advice and support during the sterols imaging. We are grateful for fruitful discussions with Liz Hambleton, with Christopher Laumer and with colleagues in the Department of Symbiosis (MPI-MM). We thank Miriam Weber, Christian Lott, and HYDRA staff for sample collections. We are grateful to the Max-Planck Society for their generous financial support over the many years it took to bring this work to fruition. M.K. acknowledges financial support from the National Institute of General Medical Sciences of the National Institutes of Health under Award Number R35GM138362 and the U.S. National Science Foundation (grant IOS 2003107). This work is contribution *XXX* from the Carrie Bow Cay Laboratory, Caribbean Coral Reef Ecosystem Program, National Museum of Natural History, Washington DC.

References

Bien, T., Hambleton, E. A., Dreisewerd, K., & Soltwisch, J. (2021). Molecular insights into symbiosis—Mapping sterols in a marine flatworm-algae-system using high spatial resolution MALDI-2-MS imaging with ion mobility separation. *Analytical and Bioanalytical Chemistry*, *413*(10), 2767–2777. https://doi.org/10.1007/s00216-020-03070-0

Bin Sayeed, M. S., & Ameen, S. S. (2015). Beta-Sitosterol: A Promising but Orphan Nutraceutical to Fight Against Cancer. *Nutrition and Cancer*, *67*(8), 1216–1222. https://doi.org/10.1080/01635581.2015.1087042

Birgel, D., Elvert, M., Han, X., & Peckmann, J. (2008). 13C-depleted biphytanic diacids as tracers of past anaerobic oxidation of methane. *Organic Geochemistry*, *39*(1), 152–156. https://doi.org/10.1016/j.orggeochem.2007.08.013

Bouvier-Navé, P., Husselstein, T., & Benveniste, P. (1998). Two families of sterol methyltransferases are involved in the first and the second methylation steps of plant sterol biosynthesis. *European Journal of Biochemistry*, *256*(1), 88–96. https://doi.org/10.1046/j.1432-1327.1998.2560088.x

Breitkopf, S., Ricoult, S., Yuan, M., Xu, Y., Peake, D., Manning, B., & Asara, J. (2017). A relative quantitative positive/negative ion switching method for untargeted lipidomics via high resolution LC-MS/MS from any biological source. *Metabolomics*, *13*. https://doi.org/10.1007/s11306-016-1157-8

Bright, M., & Giere, O. (2005). Microbial symbiosis in Annelida. *Symbiosis*, *38*(1), 1–45.

Canuel, E. A., Freeman, K. H., & Wakeham, S. G. (1997). Isotopic compositions of lipid biomarker compounds in estuarine plants and surface sediments. *Limnology and Oceanography*, *42*(7), 1570–1583. https://doi.org/10.4319/lo.1997.42.7.1570

Capella-Gutiérrez, S., Silla-Martínez, J. M., & Gabaldón, T. (2009). trimAl: A tool for automated alignment trimming in large-scale phylogenetic analyses. *Bioinformatics*, *25*(15), 1972–1973. https://doi.org/10.1093/bioinformatics/btp348

Chiang, J. Y. L., & Ferrell, J. M. (2020). Bile Acid Biology, Pathophysiology, and Therapeutics. *Clinical Liver Disease*, *15*(3), 91–94. https://doi.org/10.1002/cld.861

Chitwood, D. J. (1991). Nematode sterol biochemistry. *Physiology and Biochemistry of Sterols.*, 257–293.

Chitwood, D. J., Hutzell, P. A., & Lusby, W. R. (1985). Sterol Composition of the Corn Cyst Nematode, *Heterodera zeae*, and Corn Roots. *Journal of Nematology*, *17*(1), 64–68.

Chitwood, D. J., McClure, M. A., Feldlaufer, M. F., Lusby, W. R., & Oliver, T. E. (1987). Sterol Composition and Ecdysteroid Content of Eggs of the Root-knot Nematodes *Meloidogyne incognita* and *M. arenaria*. *Journal of Nematology*, *19*(3), 352–360.

Cole, R. J., & Krusberg, L. R. (1967). Sterol composition of the Nematodes *Ditylenchus triformis* and *Ditylenchus dipsaci*, and host tissues. *Experimental Parasitology*, *21*(2), 232–239. https://doi.org/10.1016/0014-4894(67)90085-9

Darnet, S., Fliesler, S. J., & Schaller, H. (2020). Worming our way toward multiple evolutionary origins of convergent sterol pathways. *Journal of Lipid Research*, *61*(2), 129–132. https://doi.org/10.1194/jlr.C119000600

Desmond, E., & Gribaldo, S. (2009). Phylogenomics of Sterol Synthesis: Insights into the Origin, Evolution, and Diversity of a Key Eukaryotic Feature. *Genome Biology and Evolution*, *1*, 364–381. https://doi.org/10.1093/gbe/evp036

Germer, J., Cerveau, N., & Jackson, D. J. (2017). The Holo-Transcriptome of a Calcified Early Branching Metazoan. *Frontiers in Marine Science*, *4*. https://doi.org/10.3389/fmars.2017.00081

Giere, O. (1981). The Gutless Marine Oligochaete *Phallodrilus leukodermatus*. Structural Studies on an Aberrant Tubificid Associated with Bacteria. *Marine Ecology Progress Series*, *5*, 353–357. https://doi.org/10.3354/meps005353

Giere, O. (1985). The Gutless Marine Tubificid Phallodrilus planus, a Flattened Oligochaete with Symbiotic Bacteria. Results from Morphological and Ecological Studies. *Zoologica Scripta*, *14*(4), 279–286. https://doi.org/10.1111/j.1463-6409.1985.tb00198.x

Gold, D. A., Grabenstatter, J., Mendoza, A. de, Riesgo, A., Ruiz-Trillo, I., & Summons, R. E. (2016). Sterol and genomic analyses validate the sponge biomarker hypothesis. *Proceedings of the National Academy of Sciences*, *113*(10), 2684–2689. https://doi.org/10.1073/pnas.1512614113

Guan, H., Birgel, D., Feng, D., Peckmann, J., Liu, L., Liu, L., & Tao, J. (2021). Lipids and their δ13C values reveal carbon assimilation and cycling in the methane-seep tubeworm *Paraescarpia echinospica* from the South China Sea. *Deep Sea Research Part I: Oceanographic Research Papers*, *174*, 103556. https://doi.org/10.1016/j.dsr.2021.103556

Gurevich, A., Saveliev, V., Vyahhi, N., & Tesler, G. (2013). QUAST: Quality assessment tool for genome assemblies. *Bioinformatics*, *29*(8), 1072–1075. https://doi.org/10.1093/bioinformatics/btt086

Hartmann, M.-A. (2004). 5 Sterol metabolism and functions in higher plants. In G. Daum (Ed.), *Lipid Metabolism and Membrane Biogenesis* (pp. 183–211). Springer. https://doi.org/10.1007/978-3-540-40999-1_6

Haubrich, B. A., Collins, E. K., Howard, A. L., Wang, Q., Snell, W. J., Miller, M. B., Thomas, C. D., Pleasant, S. K., & Nes, W. D. (2015). Characterization, mutagenesis and mechanistic analysis of an ancient algal sterol C24-methyltransferase: Implications for understanding sterol evolution in the green lineage. *Phytochemistry*, *113*, 64–72. https://doi.org/10.1016/j.phytochem.2014.07.019

Hayes, J. M. (2018). 3. Fractionation of Carbon and Hydrogen Isotopes in Biosynthetic Processes. In *Stable Isotope Geochemistry* (pp. 225–278). De Gruyter. https://www.degruyter.com/document/doi/10.1515/9781501508745-006/html

Hemmrich, G., & Bosch, T. C. G. (2008). Compagen, a comparative genomics platform for early branching metazoan animals, reveals early origins of genes regulating stem-cell differentiation. *BioEssays*, *30*(10), 1010–1018. https://doi.org/10.1002/bies.20813

Howe, K. L., Contreras-Moreira, B., De Silva, N., Maslen, G., Akanni, W., Allen, J., Alvarez-Jarreta, J., Barba, M., Bolser, D. M., Cambell, L., Carbajo, M., Chakiachvili, M., Christensen, M., Cummins, C., Cuzick, A., Davis, P., Fexova, S., Gall, A., George, N., … Flicek, P. (2020). Ensembl Genomes 2020—Enabling non-vertebrate genomic research. *Nucleic Acids Research*, *48*(D1), D689–D695. https://doi.org/10.1093/nar/gkz890

Jayasimha, P., & Nes, W. D. (2008). Photoaffinity Labeling and Mutational Analysis of 24-C-Sterol Methyltransferase Defines the AdoMet Binding Site. *Lipids*, *43*(8), 681–693. https://doi.org/10.1007/s11745-008-3198-x

Jensen, M., Wippler, J., & Kleiner, M. (2021). Evaluation of RNAlater™ as a field-compatible preservation method for metaproteomic analyses of bacteria-animal symbioses (p. 2021.06.16.448770). https://doi.org/10.1101/2021.06.16.448770

Kadesch, P., Quack, T., Gerbig, S., Grevelding, C. G., & Spengler, B. (2019). Lipid Topography in Schistosoma mansoni Cryosections, Revealed by Microembedding and High-Resolution Atmospheric-Pressure Matrix-Assisted Laser Desorption/Ionization (MALDI) Mass Spectrometry Imaging. *Analytical Chemistry*, *91*(7), 4520–4528. https://doi.org/10.1021/acs.analchem.8b05440

Keller, O., Odronitz, F., Stanke, M., Kollmar, M., & Waack, S. (2008). Scipio: Using protein sequences to determine the precise exon/intron structures of genes and their orthologs in closely related species. *BMC Bioinformatics*, *9*(1), 278. https://doi.org/10.1186/1471-2105-9-278

Kent, W. J. (2002). BLAT—The BLAST-Like Alignment Tool. *Genome Research*, *12*(4), 656–664. https://doi.org/10.1101/gr.229202

Kleiner, M., Wentrup, C., Holler, T., Lavik, G., Harder, J., Lott, C., Littmann, S., Kuypers, M. M. M., & Dubilier, N. (2015). Use of carbon monoxide and hydrogen by a bacteria–animal symbiosis from seagrass sediments. *Environmental Microbiology*, *17*(12), 5023–5035. https://doi.org/10.1111/1462-2920.12912

Kleiner, M., Wentrup, C., Lott, C., Teeling, H., Wetzel, S., Young, J., Chang, Y.-J., Shah, M., VerBerkmoes, N. C., Zarzycki, J., Fuchs, G., Markert, S., Hempel, K., Voigt, B., Becher, D., Liebeke, M., Lalk, M., Albrecht, D., Hecker, M., … Dubilier, N. (2012). Metaproteomics of a gutless marine worm and its symbiotic microbial community reveal unusual pathways for carbon and energy use. *Proceedings of the National Academy of Sciences*, *109*(19), E1173–E1182. https://doi.org/10.1073/pnas.1121198109

Kolmogorov, M., Yuan, J., Lin, Y., & Pevzner, P. A. (2019). Assembly of long, error-prone reads using repeat graphs. *Nature Biotechnology*, *37*(5), 540–546. https://doi.org/10.1038/s41587-019-0072-8

Lagarda, M. J., García-Llatas, G., & Farré, R. (2006). Analysis of phytosterols in foods. *Journal of Pharmaceutical and Biomedical Analysis*, *41*(5), 1486–1496. https://doi.org/10.1016/j.jpba.2006.02.052

Larkin, M. A., Blackshields, G., Brown, N. P., Chenna, R., McGettigan, P. A., McWilliam, H., Valentin, F., Wallace, I. M., Wilm, A., Lopez, R., Thompson, J. D., Gibson, T. J., & Higgins, D. G. (2007). Clustal W and Clustal X version 2.0. *Bioinformatics (Oxford, England)*, *23*(21), 2947–2948. https://doi.org/10.1093/bioinformatics/btm404

Letunic, I., & Bork, P. (2019). Interactive Tree Of Life (iTOL) v4: Recent updates and new developments. *Nucleic Acids Research*, *47*(W1), W256–W259. https://doi.org/10.1093/nar/gkz239

Li, H., Zhao, X., Wang, J., Dong, Y., Meng, S., Li, R., Niu, X., & Deng, X. (2015). β-sitosterol interacts with pneumolysin to prevent *Streptococcus pneumoniae* infection. *Scientific Reports*, *5*(1), 17668. https://doi.org/10.1038/srep17668

Luo, J., Yang, H., & Song, B.-L. (2020). Mechanisms and regulation of cholesterol homeostasis. *Nature Reviews Molecular Cell Biology*, *21*(4), 225–245. https://doi.org/10.1038/s41580-019-0190-7

McCutchan, J. H., Lewis, W. M., Kendall, C., & McGrath, C. C. (2003). Variation in trophic shift for stable isotope ratios of carbon, nitrogen, and sulfur. *Oikos*, *102*(2), 378–390. https://doi.org/10.1034/j.1600-0706.2003.12098.x

Minh, B. Q., Schmidt, H. A., Chernomor, O., Schrempf, D., Woodhams, M. D., von Haeseler, A., & Lanfear, R. (2020). IQ-TREE 2: New Models and Efficient Methods for Phylogenetic Inference in the Genomic Era. *Molecular Biology and Evolution*, *37*(5), 1530–1534. https://doi.org/10.1093/molbev/msaa015

Mouritsen, O. G., & Zuckermann, M. J. (2004). What's so special about cholesterol? *Lipids*, *39*(11), 1101–1113. https://doi.org/10.1007/s11745-004-1336-x

Najle, S. R., Molina, M. C., Ruiz-Trillo, I., & Uttaro, A. D. (2016). Sterol metabolism in the filasterean *Capsaspora owczarzaki* has features that resemble both fungi and animals. *Open Biology*, *6*(7), 160029. https://doi.org/10.1098/rsob.160029

Neelakandan, A. K., Song, Z., Wang, J., Richards, M. H., Wu, X., Valliyodan, B., Nguyen, H. T., & Nes, W. D. (2009). Cloning, functional expression and phylogenetic analysis of plant sterol 24C-methyltransferases involved in sitosterol biosynthesis. *Phytochemistry*, *70*(17), 1982–1998. https://doi.org/10.1016/j.phytochem.2009.09.003

Nes, W. D., & Heupel, R. C. (1986). Physiological requirement for biosynthesis of multiple 24β-methyl sterols in *Gibberella fujikuroi*. *Archives of Biochemistry and Biophysics*, *244*(1), 211–217. https://doi.org/10.1016/0003-9861(86)90110-4

Nes, W. D., Jayasimha, P., & Song, Z. (2008). Yeast sterol C24-methyltransferase: Role of highly conserved tyrosine-81 in catalytic competence studied by site-directed mutagenesis and thermodynamic analysis. *Archives of Biochemistry and Biophysics*, *477*(2), 313–323. https://doi.org/10.1016/j.abb.2008.05.016

Nes, W. D., Jayasimha, P., Zhou, W., Kanagasabai, R., Jin, C., Jaradat, T. T., Shaw, R. W., & Bujnicki, J. M. (2004). Sterol Methyltransferase: Functional Analysis of Highly Conserved Residues by Site-Directed Mutagenesis. *Biochemistry*, *43*(2), 569–576. https://doi.org/10.1021/bi035257z

Phleger, C. F., Nelson, M. M., Groce, A. K., Cary, S. C., Coyne, K. J., & Nichols, P. D. (2005). Lipid composition of deep-sea hydrothermal vent tubeworm *Riftia pachyptila*, crabs *Munidopsis subsquamosa* and *Bythograea thermydron*, mussels *Bathymodiolus sp.* And limpets *Lepetodrilus spp. Comparative Biochemistry and Physiology Part B: Biochemistry and Molecular Biology*, *141*(2), 196–210. https://doi.org/10.1016/j.cbpc.2005.03.001

Radhakrishnan, A., Rohatgi, R., & Siebold, C. (2020). Cholesterol access in cellular membranes controls Hedgehog signaling. *Nature Chemical Biology*, *16*(12), 1303–1313. https://doi.org/10.1038/s41589-020-00678-2

Rieley, G., Dover, C. L. van, Hedrick, D. B., White, D. C., & Eglinton, G. (1995). Lipid characteristics of hydrothermal vent organisms from 9°N, East Pacific Rise. *Geological Society, London, Special Publications*, *87*(1), 329–342. https://doi.org/10.1144/GSL.SP.1995.087.01.25

Saeidnia, S., Manayi, A., Gohari, A. R., & Abdollahi, M. (2014). The story of beta-sitosterol-a review. *European Journal of Medicinal Plants*, *4*(5), 590.

Sarkar, P., & Chattopadhyay, A. (2022). Cholesterol in GPCR Structures: Prevalence and Relevance. *The Journal of Membrane Biology*, *255*(1), 99–106. https://doi.org/10.1007/s00232-021-00197-8

Schaller, H. (2004). New aspects of sterol biosynthesis in growth and development of higher plants. *Plant Physiology and Biochemistry*, *42*(6), 465–476. https://doi.org/10.1016/j.plaphy.2004.05.012

Seppey, M., Manni, M., & Zdobnov, E. M. (2019). BUSCO: Assessing Genome Assembly and Annotation Completeness. *Methods in Molecular Biology (Clifton, N.J.)*, *1962*, 227–245. https://doi.org/10.1007/978-1-4939-9173-0_14

Shi, C., Wu, F., & Xu, J. (2013). Incorporation of β-sitosterol into mitochondrial membrane enhances mitochondrial function by promoting inner mitochondrial membrane fluidity. *Journal of Bioenergetics and Biomembranes*, *45*(3), 301–305. https://doi.org/10.1007/s10863-012-9495-3

Simons, K., & Ikonen, E. (1997). Functional rafts in cell membranes. *Nature*, *387*(6633), 569–572. https://doi.org/10.1038/42408

Simons, K., & Toomre, D. (2000). Lipid rafts and signal transduction. *Nature Reviews Molecular Cell Biology*, *1*(1), 31–39. https://doi.org/10.1038/35036052

Soltwisch, J., Heijs, B., Koch, A., Vens-Cappell, S., Höhndorf, J., & Dreisewerd, K. (2020). MALDI-2 on a Trapped Ion Mobility Quadrupole Time-of-Flight Instrument for Rapid Mass Spectrometry Imaging and Ion Mobility Separation of Complex Lipid Profiles. *Analytical Chemistry*, *92*(13), 8697–8703. https://doi.org/10.1021/acs.analchem.0c01747

Spivak, M., Weston, J., Bottou, L., Käll, L., & Noble, W. S. (2009). Improvements to the Percolator Algorithm for Peptide Identification from Shotgun Proteomics Data Sets. *Journal of Proteome Research*, *8*(7), 3737–3745. https://doi.org/10.1021/pr801109k

Studier, F. W. (2005). Protein production by auto-induction in high-density shaking cultures. *Protein Expression and Purification*, *41*(1), 207–234. https://doi.org/10.1016/j.pep.2005.01.016

Summons, R. E., Bradley, A. S., Jahnke, L. L., & Waldbauer, J. R. (2006). Steroids, triterpenoids and molecular oxygen. *Philosophical Transactions of the Royal Society B: Biological Sciences*, *361*(1470), 951–968. https://doi.org/10.1098/rstb.2006.1837

Summons, R. E., Welander, P. V., & Gold, D. A. (2022). Lipid biomarkers: Molecular tools for illuminating the history of microbial life. *Nature Reviews Microbiology*, *20*(3), 174–185. https://doi.org/10.1038/s41579-021-00636-2

Thummel, C. S., & Chory, J. (2002). Steroid signaling in plants and insects—Common themes, different pathways. *Genes & Development*, *16*(24), 3113–3129. https://doi.org/10.1101/gad.1042102

Tiunov, A. V. (2007). Stable isotopes of carbon and nitrogen in soil ecological studies. *Biology Bulletin*, *34*(4), 395–407. https://doi.org/10.1134/S1062359007040127

van der Meer-Janssen, Y. P. M., van Galen, J., Batenburg, J. J., & Helms, J. B. (2010). Lipids in host–pathogen interactions: Pathogens exploit the complexity of the host cell lipidome. *Progress in Lipid Research*, *49*(1), 1–26. https://doi.org/10.1016/j.plipres.2009.07.003

Veeramachaneni, P. P. (2005). Active site mapping of yeast recombinant sterol methyltransferase (Y81 W) from *Saccharomyces cerevisiae* and inhibition of ergosterol biosynthesis in *Candida albicans*. [Master Thesis]. Texas Tech University Lubbock.

Vizcaíno, J. A., Csordas, A., del-Toro, N., Dianes, J. A., Griss, J., Lavidas, I., Mayer, G., Perez-Riverol, Y., Reisinger, F., Ternent, T., Xu, Q.-W., Wang, R., & Hermjakob, H. (2016). 2016 update of the PRIDE database and its related tools. *Nucleic Acids Research*, *44*(D1), D447–D456. https://doi.org/10.1093/nar/gkv1145

Volkman, J. K. (2005). Sterols and other triterpenoids: Source specificity and evolution of biosynthetic pathways. *Organic Geochemistry*, *36*(2), 139–159. https://doi.org/10.1016/j.orggeochem.2004.06.013

Wippler, J., Kleiner, M., Lott, C., Gruhl, A., Abraham, P. E., Giannone, R. J., Young, J. C., Hettich, R. L., & Dubilier, N. (2016). Transcriptomic and proteomic insights into innate immunity and adaptations to a symbiotic lifestyle in the gutless marine worm *Olavius algarvensis*. *BMC Genomics*, *17*(1), 942. https://doi.org/10.1186/s12864-016-3293-y

Wollam, J., & Antebi, A. (2011). Sterol Regulation of Metabolism, Homeostasis, and Development. *Annual Review of Biochemistry*, *80*(1), 885–916. https://doi.org/10.1146/annurev-biochem-081308-165917

Woyke, T., Teeling, H., Ivanova, N. N., Huntemann, M., Richter, M., Gloeckner, F. O., Boffelli, D., Anderson, I. J., Barry, K. W., Shapiro, H. J., Szeto, E., Kyrpides, N. C., Mussmann, M., Amann, R., Bergin, C., Ruehland, C., Rubin, E. M., & Dubilier, N. (2006). Symbiosis

insights through metagenomic analysis of a microbial consortium. *Nature*, *443*(7114), 950–955. https://doi.org/10.1038/nature05192

Yeagle, P. L. (1985). Cholesterol and the cell membrane. *Biochimica et Biophysica Acta (BBA) - Reviews on Biomembranes*, *822*(3), 267–287. https://doi.org/10.1016/0304-4157(85)90011-5